The mechanical scaling of coasting in zebrafish (Danio rerio)

The Journal of Experimental Biology 208, 2289-2301
Published by The Company of Biologists 2005
doi:10.1242/jeb.01642

The mechanical scaling of coasting in zebrafish (*Danio rerio*)

Matthew J. McHenry[1,*] and George V. Lauder[2]

[1]*Department of Ecology and Evolutionary Biology, University of California, 321 Steinhaus Hall, Irvine, CA 92697, USA* and [2]*Department of Organismic and Evolutionary Biology, Harvard University, 26 Oxford Street, Cambridge, MA 02138, USA*

*Author for correspondence (e-mail: mmchenry@uci.edu)

Accepted 11 April 2005

Summary

Many fish species span two or three orders of magnitude in length during the growth from larvae to adults, and this change may have dramatic consequences for locomotor performance. We measured how the performance of coasting changes over the life history of zebrafish (*Danio rerio*) and examined the scaling of mechanics underlying this change. Adult zebrafish coast disproportionately further and faster and maintain their speed for a longer duration than do larvae and juveniles. Measurements of drag on tethered dead fish suggest that adult fish operate in an inertial regime by coasting at relatively high Reynolds numbers (*Re*>1000), and *in vivo* drag measurements showed adults to operate with a drag coefficient ($C_{inert}\approx0.024$) that was consistent with previously published estimates. However, drag scaled differently at lower *Re* values than those assumed in previous studies. We found a viscous regime at *Re*<300, which corresponds to the routine coasting of larvae and juveniles. Despite these changes in hydrodynamics over growth, a mathematical model of coasting mechanics suggests that the disproportionately longer coasting of adults is caused primarily by their large body mass and high speed at the beginning of coasting. We therefore propose that changes in coasting performance with growth are dictated primarily by the scaling of momentum rather than resulting from hydrodynamic changes. These results provide an opportunity for new interpretations of function in the growth and evolution of fish.

Key words: gliding, locomotion, swimming, fish.

Introduction

The size of a swimming organism has important consequences for the hydrodynamic resistance to its motion. Microorganisms act against the viscosity of water, while animals greater than a few centimetres in length must overcome an uneven distribution in pressure along the surface of the body (Daniel et al., 1992; Videler et al., 2002; Wu, 1977). For the tremendous diversity of animals at a scale intermediate to these body sizes, it remains unclear to what degree viscous and inertial forces contribute to drag during locomotion (Fuiman and Batty, 1997; McHenry et al., 2003; Muller et al., 2000). Zebrafish (*Danio rerio*) grow from a length of a few millimetres as larvae to a few centimetres as adults and therefore provide a model system for examining the locomotor mechanics of this intermediate scale. Like many fish species, zebrafish swim intermittently and thus spend at least half of a locomotory period coasting passively (i.e. maintaining a stretched straight posture while moving forward) against the surrounding water (Fuiman and Webb, 1988). The goals of the present study were to examine how the mechanics of coasting scale with size and to consider how these changes influence locomotor performance over the life history of zebrafish.

The scaling of drag

The ratio of viscous to inertial drag is proportional to the Reynolds number (*Re*) of an animal, but this proportionality cannot easily be estimated by hydrodynamic theory and therefore requires measurements to be understood. In order to measure the relationship between drag and Reynolds number $Re=\rho UL/\mu$, where U is swimming speed, L is body length, and ρ and μ are, respectively, the density and dynamic viscosity of water: Lamb, 1945), *Re* may be varied by changing the speed of flow past the body or altering the density or viscosity of the fluid. At high *Re*, inertial drag is predicted to vary with water density, the square of the swimming speed and the wetted area of the body (S; Batchelor, 1967). Therefore, measured drag, D, normalized by these terms yields the inertial drag coefficient, C_{inert} (most commonly denoted as C_d; Batchelor, 1967), which is predicted to remain constant with respect to *Re* when inertia dominates:

$$C_{inert} = (2D)/(\rho SU^2). \quad (1)$$

In contrast, viscous drag varies with body length, the viscosity of water and speed (Lamb, 1945), so measurements of drag normalized by these terms provides a viscous drag

coefficient, C_{visc}, that is predicted to remain constant with respect to *Re* in a viscous-dominated regime:

$$C_{visc} = D/(L\mu U). \quad (2)$$

Both measurements of non-dimensional drag are expected to vary with *Re* if drag is generated by a combination of viscous and inertial forces. Therefore, measurements of these coefficients over a range of *Re* may be used to identify viscous, inertial and intermediate regimes and thereby define the scaling of drag for a particular animal. The present study used this approach to define the scaling of drag in zebrafish.

Ontogenetic change in behaviour and performance

The scaling of drag provides a means for interpreting ontogenetic changes in the behaviour of fish. Weihs (1980) proposed that anchovy (*Engraulis mordax*) operate in a viscous regime as larvae swimming at *Re*<10 and an inertial regime as adults at *Re*>200. It followed that during the growth between these stages, inertial forces increasingly played a dominant role in the hydrodynamics of swimming. This scaling was consistent with measurements of drag for bluff bodies (e.g. the sphere and cylinder) at comparable *Re* values (where few measurements existed for streamlined bodies; Hoerner, 1965) and it provided the fundamental set of assumptions for a mathematical model of ontogenetic change in swimming mechanics (Weihs, 1980). The results of this model suggested that larval anchovy conserve energy by switching from a steady to an intermittent swimming behaviour (Hunter, 1972) upon growing to a size where they operate outside of the proposed viscous regime (*Re*>10; Weihs, 1980). It is at this transition that other species of juvenile fish adopt foraging behaviours that were considered to benefit from the low energetic cost of intermittent motion in an inertial environment (Webb and Weihs, 1986). At this stage in their life history, zebrafish are capable of changing their direction of swimming to an equal or greater extent than the earlier larval stage despite using their paired fins less and beating their tails with lower curvature. These kinematics give juvenile fish the appearance of greater manoeuvrability than larvae (Budick and O'Malley, 2000; Fuiman and Webb, 1988; Muller and van Leeuwen, 2004; Thorsen et al., 2004).

The hydrodynamic scaling proposed by Weihs (1980) has also provided a basis for interpretations of ontogenetic change in morphology. For example, the elongated body of larval fish in many species is thought to contribute to their ability to exit precociously from the viscous regime by having a greater body length than if they possessed the compressed body shapes typical of adults (Muller and Videler, 1996; Osse, 1990; Webb and Weihs, 1986). It is subsequent to growing out of the viscous regime that many species assume a streamlined body shape that reduces pressure drag in an inertial hydrodynamic environment.

Fuiman and Batty (1997) presented one of the few experimental tests of the hydrodynamic scaling used to interpret the functional consequences of changes in morphology and behaviour. They found a linear correlation between stride length (i.e. the distanced traversed by the body in one half tailbeat) and the viscous drag product ($UL\mu$) in larval herring (*Clupea harangus*) at *Re*<300 but found that the relationship became disrupted at *Re*>300. These results were interpreted as evidence that the viscous regime extends into Reynolds numbers that are greater than an order of magnitude above that proposed by Weihs (1980). However, Fuiman and Batty (1997) did not offer *a priori* predictions for the relationship between stride length and the viscous drag product or for the effect of inertial forces based on hydrodynamic theory. It is therefore unclear if the disruption between stride length and the viscous drag product was due to alterations in hydrodynamics or the result of other changes, such as the pattern of midline kinematics (which vary with size and speed in other species; Muller and van Leeuwen, 2004). Therefore, it remains unclear if the results of Fuiman and Batty (1997) present a challenge to the hydrodynamic scaling proposed by Weihs (1980).

Drag measurements

Biologists and engineers remain challenged by the question of how best to measure the drag experienced by a swimming animal. This area of biomechanics has shifted from the use of kinematics, direct force measurements of dead animals and analytical modelling (reviewed by Blake, 1983; Videler, 1993; Webb, 1975) in favour of digital flow visualization (e.g. Anderson et al., 2001; Drucker and Lauder, 1997) and computational fluid dynamics (e.g. Liu et al., 1996; Wolfgang et al., 1999) to estimate drag (Schultz and Webb, 2002). Proponents of these relatively new techniques have emphasized the need to independently validate novel experimental and theoretical approaches (e.g. Drucker and Lauder, 1999; Liu et al., 1997), yet there are few direct or indirect measurements of drag at the *Re* scale where larval and juvenile fish operate.

Drag is most directly measured with a force transducer attached to a dead fish that is exposed to flow. Although the force measured in such a 'dead drag' experiment (Webb, 1975) is unlike the drag experienced by an undulating body (Anderson et al., 2001; Lighthill, 1971; Schultz and Webb, 2002), it may approximate the drag on a coasting fish (or one propelled by paired fins with low-amplitude oscillations; Drucker and Lauder, 1999) under a few assumptions. Specifically, these measurements require that differences in the surface properties, body posture and motion of the fins between the dead and coasting fish have a relatively small effect on the total drag generated by the body. Concerns about these assumptions, along with the potential for experimental artefacts generated by fin fluttering or tethering the body at an erroneous angle of attack, are cause for scepticism about the accuracy of dead drag measurements (see Blake, 1983; Schultz and Webb, 2002; Videler, 1993; Webb, 1975).

Indirect measurements of drag from kinematics provide an alternative to the dead drag approach but introduce other assumptions and sources of error. Because drag is the sum total of hydrodynamic forces acting in opposition to the body motion of a coasting animal, it should be equivalent to the product of body mass and the average rate of deceleration and therefore may be calculated from measurements of mass and

the kinematics of coasting (Clark and Bemis, 1979; Lang and Daybell, 1963; Videler, 1981). However, calculating the drag coefficient in this manner from video recordings is susceptible to large experimental error. Differentiating position measurements twice to yield acceleration generates a low signal-to-noise ratio (Lathi, 1998; Walker, 1998), which is compounded by dividing these values by the square of velocity (found by differentiating position once) to calculate the inertial drag coefficient (Eqn 1). Furthermore, such measurements of drag coefficient have generally been based on only a single pair of velocity estimates from the coasting period. To address these concerns, Bilo and Nachtigall (1980) estimated the drag coefficient for a penguin by fitting the first integral of the equation of motion to velocity measurements. This method offered an improvement over the use of acceleration measurements by requiring only a single differentiation of positional recordings and by using the entire time series of data for a coasting sequence to calculate a single coefficient value. However, this approach assumes that the animal maintains a fixed posture and a high enough *Re* to remain in the inertial regime throughout the coast. Therefore, applying the Bilo and Nachtigall (1980) approach to juvenile and larval fish is tenuous because it is possible that these animals operate in the viscous or intermediate regimes.

The present study used a combination of dead drag and *in vivo* drag measurements to examine changes in the hydrodynamics of coasting over ontogeny. Dead drag measurements have the advantage of being applicable at any *Re* value. We therefore used this method to define viscous, inertial and intermediate regimes. We did not expect experimental errors in these measurements (Videler, 1993; Webb, 1975) to approach the magnitude of the effect of hydrodynamic scaling (Hoerner, 1965). However, we tested the accuracy of the dead drag approach with measurements of *in vivo* drag on coasting adult fish that could safely be assumed to operate in the inertial regime (Muller et al., 2000).

The present study

Intermittent swimming may be considered in terms of a periodic building up of momentum during propulsion that is followed by its loss during coasting. The ability of a fish to cover distance and maintain speed during a coast depends not only on its rate of momentum loss (i.e. drag) but also on the momentum gained during the propulsive phase. Therefore, the present study considered the scaling of both drag and momentum on the coasting performance of zebrafish. This work focused on addressing the following questions: (1) how does coasting performance change with size; (2) how do the hydrodynamics of coasting change with size and (3) how does the scaling of drag and momentum affect performance?

Materials and methods

The body dimensions, motion and biomechanics of zebrafish were measured at different stages of growth. These fish ranged in size from larvae with newly inflated swim bladders (~5 days post-fertilization and ~4.2 mm in body length) to mature adults (>90 days post-fertilization, ~45 mm in length). All wild-type *Danio rerio* Hamilton 1922 were maintained according to standard protocols (Westerfield, 1995) on a 14 h:10 h light:dark cycle at 26°C.

Coasting kinematics

We measured the kinematics of coasting from video recordings of routine swimming in fish over the full range of growth stages. In order to automate measurements of body position, high-contrast images of the body's silhouette were produced by illuminating the translucent acrylic floor of the

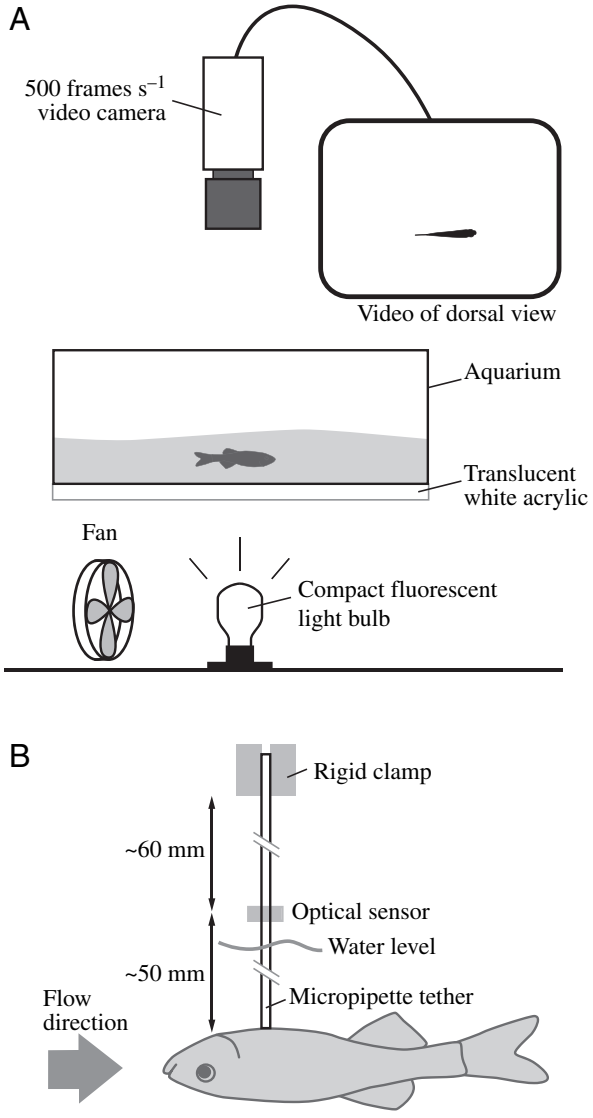

Fig. 1. Experimental setup. (A) The routine swimming of zebrafish was recorded from a dorsal perspective with high-speed video. High-contrast video images were generated by illuminating the translucent floor of the aquarium with a fluorescent light, which was prevented from heating the floor of the tank by the use of a computer fan. (B) Drag was measured by tethering dead fish from the ventral surface and exposing the body to flow (see text for details).

aquarium with a compact florescent light bulb (40 W; Greenlite, Irvine, CA, USA). The water temperature during experiments was maintained between 25°C and 26°C by cooling the light source with a computer fan (12 V; Fig. 1A). Coasting was recorded with high-resolution, high-speed digital video (500 frames s^{-1} at 1280×1024 pixels) with the camera (NAC Hi-Dcam II) focused on the centre of the aquarium using a macro lens (50 mm Nikkor, Nikon, Tokyo, Japan) with a field of view ranging from ~4 mm to ~50 mm in width. The eyes of the zebrafish appeared as the darkest pixels in video frames and thereby provided a consistent pair of landmarks that were tracked by a custom image-processing program (written in Matlab 6.0; Mathworks). The position of the caudal peduncle was acquired by manual tracking within this Matlab program.

Kinematic variables were calculated from measurements of cranial position and orientation and body posture. The cranial position was taken as the centre point between a fish's eyes, and its orientation, θ, was perpendicular to the axis between the centres of the eyes and directed anteriorly. The body posture was measured by the caudal position, φ, which is the angle between the orientation of the cranium and the position of the caudal peduncle. The coast phase was considered to be the period when φ maintained a constant zero value, but ended if the body ceased to move forward. Coasting sequences were rejected for analysis if fish visibly moved their fins.

Kinematic parameters describing coasting were found by non-linear curve fitting kinematic equations to cranial position measurements. The temporal changes in speed, U, were approximated as an asymptotic decay towards zero:

$$U(t) = U_0\, e^{-t/\tau}, \quad (3)$$

where U_0 is the initial speed and τ is a time constant that expresses the ability of a fish to maintain speed. Integrating this equation with respect to time yields an equation describing cranial position, x, with a zero initial value:

$$x(t) = U_0\, \tau(1 - e^{-t/\tau}). \quad (4)$$

Values for U_0 and τ were found by a non-linear least-squares curve fit of this equation to position measurements (Gauss-Newton method in Matlab). In order to correct for behavioural variation in coast duration, the coast distance, d, was calculated with Eqn 4 as the distance traversed in the mean coast duration for all fish. Therefore, the performance of each coast was characterized by the kinematic parameters d, τ and U_0.

Drag measurements

The scaling of drag was characterized from measurements of drag coefficients for adult fish over a range of *Re*. For these experiments, fish were euthanized by an overdose of MS-222 (Argent, Chemical Laboratories, Redmond, WA, USA) and fixed in a 10% formalin solution overnight to stiffen the body and fins. During fixation, the body was turned upside down and supported on the dorsal surface with wires that did not touch the fins. This arrangement allowed the fins to be fixed in their resting posture, with the pectoral fins approximately aligned with the frontal plane of the body and the median fins flattened along the sagittal plane. During experiments, fish were attached by their ventral surface to a glass micropipette (50 µl microcaps; Drummond Scientific, Broomall, PA, USA), using light suction (as in McHenry and Strother, 2003), and oriented toward flow in a flow tank (Fig. 1B) by adjusting the pitch and yaw of the body by eye. The fixed bodies of fish were sufficiently rigid that no fluttering by the fins was observed. Deflection of the micropipette was recorded with an optical strain gauge (11-04-001; UDT Sensors, Hawthorne, CA, USA) and calibrated for force after each drag measurement. This calibration consisted of finding the relationship between the output voltage for the strain gauge and force by rotating the apparatus to a horizontal orientation and hanging weights at the tip of the tether. The relationship between voltage and force was linear within the range of strains observed during experiments. We subtracted the drag acting on the tether from the total drag from measurements taken after releasing the fish's body from the tether. The accuracy of our experimental approach was confirmed by comparing drag measurements for a sphere with published values (White, 1991). Reynolds number was varied in these experiments by altering the viscosity of water (as in Johnston et al., 1998) through the addition of up to 8% Dextran 500 (Amersham Biosciences, Piscataway, NJ, USA) and controlling the speed of flow in our gravity-fed flow tank (from 0.9 mm s^{-1} to 60.7 mm s^{-1}). Drag on each fish was measured at six *Re* values ranging from 1 to 10,000. For each measurement, we calculated the non-dimensional drag coefficients using Eqns 1, 2. The inertial hydrodynamic regime was defined as the range of *Re* values where the inertial drag coefficient, C_{inert} (Eqn 1), remained constant with respect to *Re*. The viscous regime was defined as the range of *Re* values where the viscous drag coefficient, C_{visc} (Eqn 2), maintained a constant value, and the intermediate regime was taken as the range between viscous and inertial regimes.

The accuracy of dead drag measurements was tested with *in vivo* drag measurements of coasting fish. We found the inertial drag coefficient using the equation for the inverse of the first integral of the equation of motion for a gliding animal (Bilo and Nachtigall, 1980):

$$1/U(t) = ht + (1/U_0). \quad (5)$$

The slope of this line, h, was found by a linear least-squares curve fit to the inverse of instantaneous measurements of speed throughout a coasting sequence, with an intercept equal to the inverse of the initial speed. The inertial drag coefficient was found from this slope with the following relationship (Bilo and Nachtigall, 1980):

$$C_{inert} = (2hm)/(S\rho), \quad (6)$$

where m is body mass. Since this method requires that the fish operate in an inertial regime, we used only sequences of coasting adult fish at *Re*>1000.

Morphometrics

The size of zebrafish bodies was measured from high-

Table 1. *Morphometrics*

Growth stage	*N*	*L* (mm)	*S* (mm^2)	*V* (mm^3)	*m* (mg)
Small larva	3	4.35±0.09	7.89±1.29	1.52±0.42	0.492±0.097
Large larva	3	8.19±1.21	30.6±10.6	12.6±6.9	3.50±1.60
Juvenile	3	14.3±2.7	96.1±39.5	69.1±41.7	18.5±11.1
Adult	3	35.4±8.9	777±452	1980±1720	485±400

L, body length; *S*, wetted surface area; *V*, body volume; *m*, body mass.
Values are means ± 1 S.D.

contrast photographs of dorsal and lateral views. From these photographs, the peripheral shape of the body was traced with an automated program (in Matlab), and the body was reconstructed in three dimensions under the assumption of an elliptical shape in the transverse plane. The wetted surface area was calculated as the sum of area of polygonal elements describing the peripheral body shape, and the volume was calculated as the space enclosed by this surface (as in McHenry, 2001; McHenry et al., 2003).

Mathematical modelling

The equations of motion for fish coasting in the viscous and inertial regimes were used to examine the effects of scaling in hydrodynamics and momentum on coasting performance. We used the following equation of motion to model coasting in the inertial regime:

$$ma + A\rho Va + 0.5C_{\text{inert}}\rho SU^2 = 0 \quad (7)$$

where a is body acceleration, V is body volume, and A is the added mass coefficient. It was assumed that a zebrafish's body possesses an added mass coefficient equal to a 1:6 ellipsoid (where A=0.045; Johansson, 2003; Kochin, 1964; Munk, 1922). This equation may be solved analytically to generate a prediction of changes in body position, x, as a function of time:

$$x(t) = b\ \ln\{[(U_0 t)/b] + 1\}, \quad (8)$$

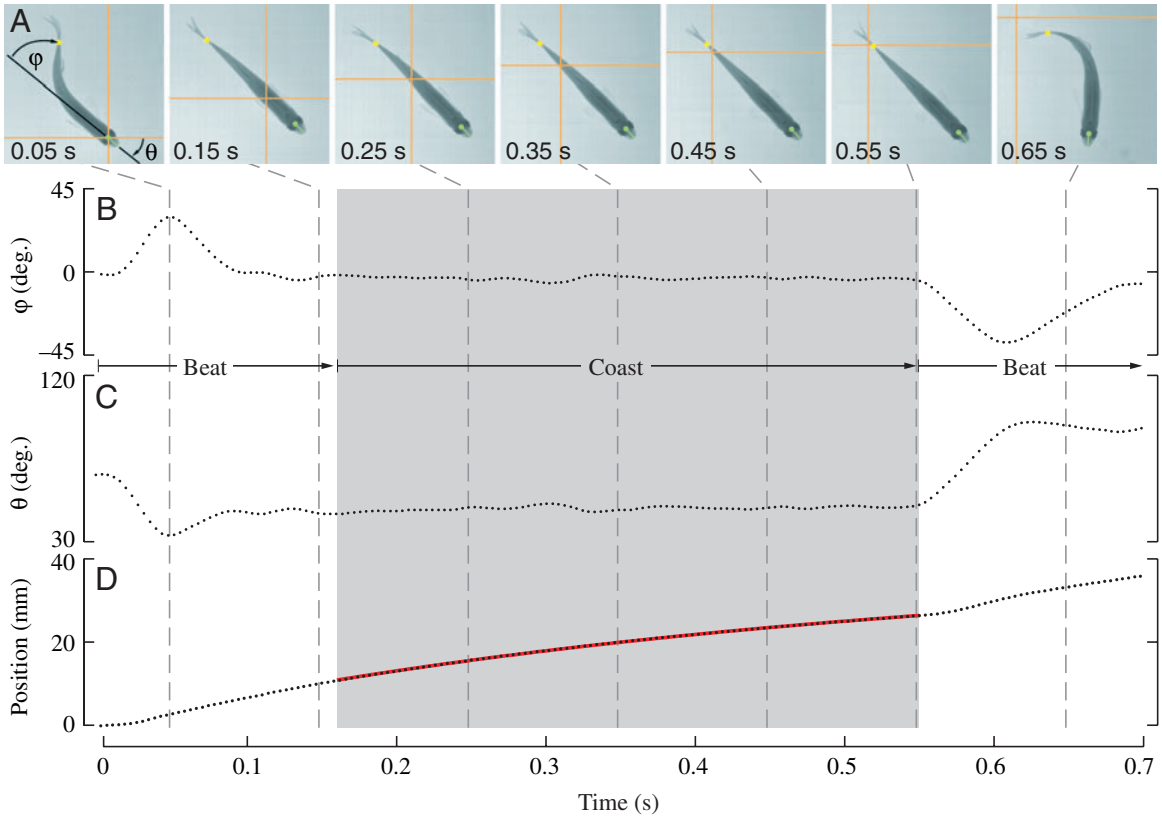

Fig. 2. Intermittent kinematics typical of the routine swimming of zebrafish. (A) Video frames at 0.10 s intervals illustrate the changes in body shape that occur during beat and coast phases of this adult (L=30.2 mm). Orange lines denote the cranial position in the first video frame, which travels along the body as the fish moves forward. The cranial orientation (θ) and angular fin position (φ) are illustrated in the first frame. (B) Fin position (φ) reflects the posture of the body during beat (white bars) and coast (gray bar) phases. (C) Body rotation is shown by changes in cranial orientation (θ) during the beat phase. (D) Measurements of the cranial position during coasting were used for non-linear curve fitting of Eqn 4 (red line) in order to calculate the initial speed, time constant and coasting distance.

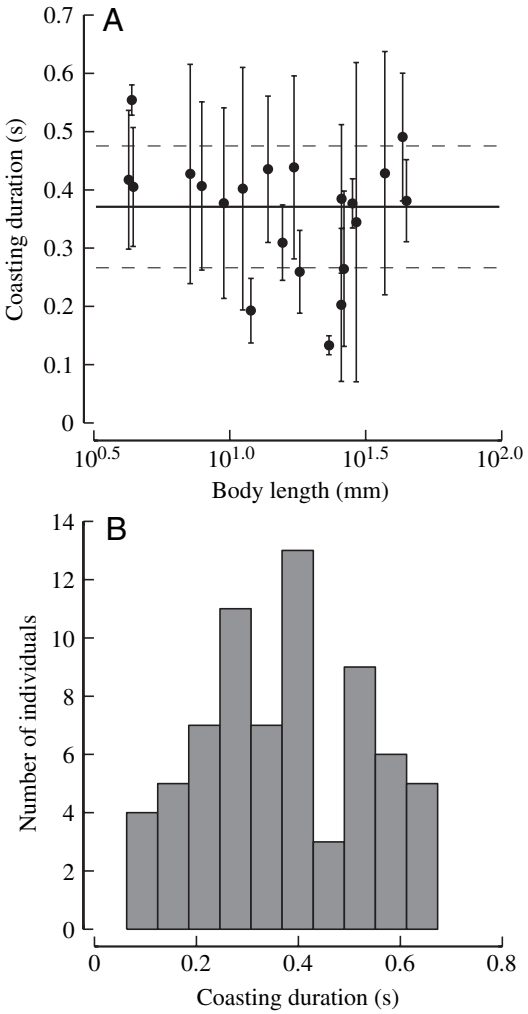

Fig. 3. The duration of the coasting phase. (A) Mean coasting duration (filled circles) and distribution (± 1 S.D.) among three coasts for individuals of different body length (N=21). The horizontal solid line shows the mean for all individuals, and the broken lines denote the distribution (± 1 S.D.) about the mean. (B) The distribution of coasting durations for 70 coasts for fish of all body lengths (N=21).

where

$$b = (2m)/(C_{\text{inert}}S\rho). \quad (9)$$

Coasting in the viscous regime has a similar form to Eqn 7 but includes a term for viscous instead of inertial drag:

$$ma + A\rho Va + C_{\text{visc}}L\mu U = 0. \quad (10)$$

The analytical solution to this equation is equivalent to Eqn 4, where:

$$\tau = (m + A\rho V)/(C_{\text{visc}}L\mu). \quad (11)$$

Mathematical simulations consisted of calculating positional changes with Eqns 4 and 8 using the measured drag coefficients from tethering experiments and the mean morphometric measurements for the small larvae, large larvae, juveniles and adults (Table 1). By using drag measurements for adults only, this approach assumed that morphological differences influenced drag coefficient to a smaller degree than did differences in *Re*. Simulations including acceleration reaction ($A\rho Va$) were compared with simulations that excluded that term in order to examine the effects of added mass. We focused on the transition between juvenile and adult stages by running a series of simulations that varied individual parameters for body size (i.e. L or S), hydrodynamic regime (i.e. Eqns 4 or 8), body mass and initial speed. These simulations were calculated for durations equal to the mean of measured coast periods, the mean + 1 S.D. and the mean – 1 S.D. in order to examine the effect of coast duration.

Results

The scaling of coasting kinematics

Zebrafish at all stages of growth routinely swam with intermittent beat and coast phases. Caudal position and cranial orientation oscillated rapidly during tail beating but maintained relatively constant values during the coast phase (Fig. 2A–C). The coefficient of determination was high (r^2>0.98) for curve fitting Eqn 4 to position measurements at all stages of growth (Fig. 2D), which suggests that this equation characterizes the kinematics of coasting well.

The duration of coasts varied greatly at all stages of growth and did not correlate with body length. For example, one small larva (L=4.25 mm) coasted for durations of 0.30 s, 0.42 s and 0.54 s and one adult (L=37.2 mm) coasted for durations of 0.20 s, 0.49 s and 0.60 s (Fig. 3A). This apparent lack of a size effect was supported by a linear regression between body length and mean coast duration that was not statistically significant (P=0.42, reduced major axis regression; Sokal and Rohlf, 1995). The distribution of coast duration was therefore approximated by the mean (μ_T=0.37 with 95% confidence intervals of L_1=0.33 and L_2=0.42) and the standard deviation (σ_T=0.10 with 95% confidence intervals of L_1=0.08 and L_2=0.15; Fig. 3B) for all individuals (N=21).

We found that the size of a fish strongly influenced its coasting kinematics. For example, one representative larva traversed a mean coasting distance (d) of less than 20% of its small body length (L=4.38 mm) whereas an adult (L=36.9 mm) coasted for more than 50% of its much larger body (Fig. 4A–C). Furthermore, adults sometimes achieved coasting distances in excess of two body lengths, and the mean coasting distance of fish larger than 23.0 mm (d=0.97L; N=9) was more than three times the mean distance of smaller fish (d=0.31L; N=12; Fig. 4D). This variation in coasting distance may be attributed to the scaling of initial speed (Fig. 4E) and the time constant (Fig. 4F) because all distances were calculated with the same period (t=0.37 s) using Eqn 4. The mechanics that account for the ability of adult fish to coast disproportionately further than larvae and juveniles were investigated in the remainder of this study.

The scaling of hydrodynamics and momentum

Viscous and inertial hydrodynamic regimes were evaluated from dead drag measurements over a range of *Re* values

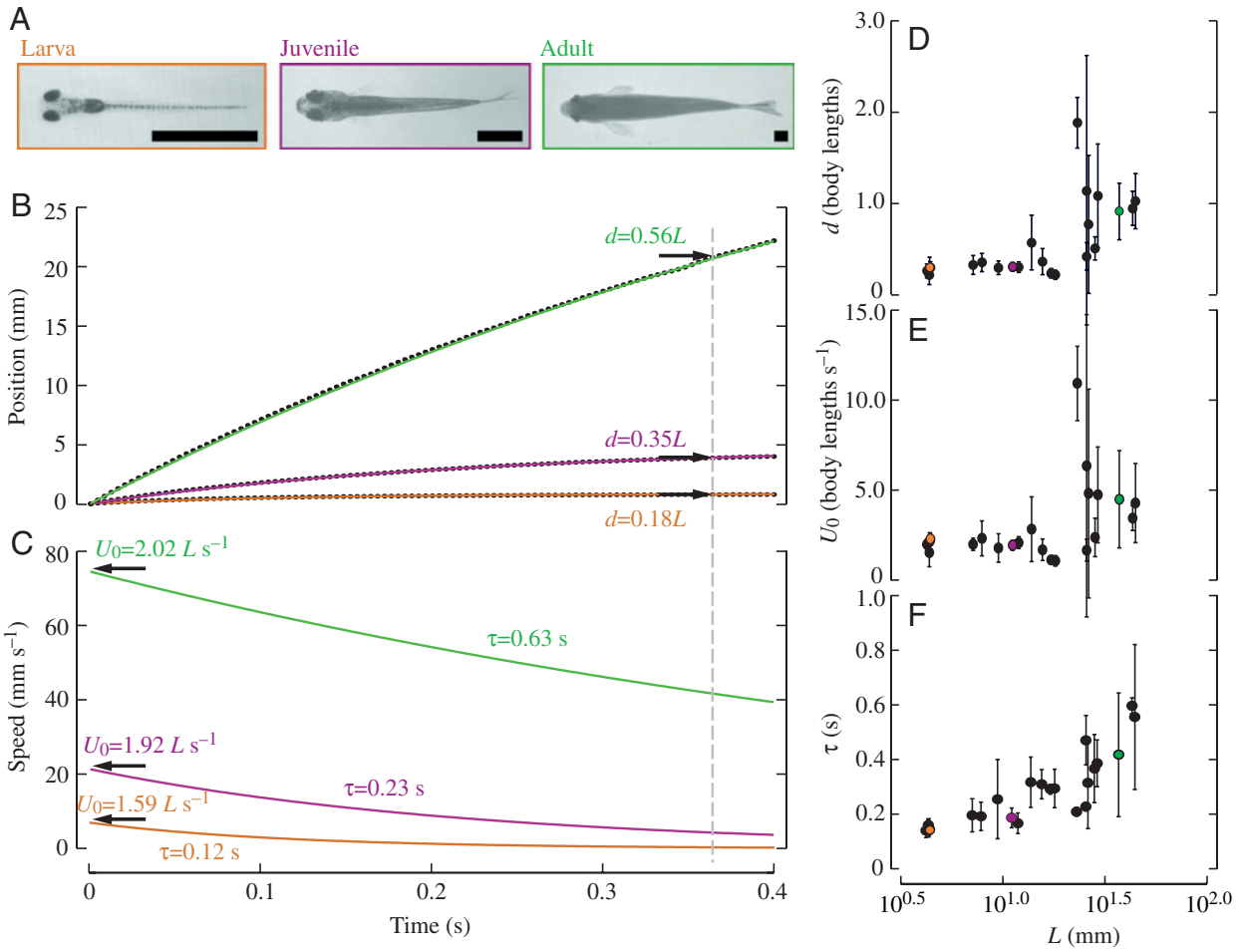

Fig. 4. The scaling of coasting performance in zebrafish. (A) Video frames of a larva (orange border), juvenile (purple border) and adult (green border) illustrate the difference in size and shape of three stages. Scale bars, 2 mm. (B) The position function (Eqn 4; coloured lines) fit to measurements of body position (filled circles; down-sampled for clarity) provided measurements of the time constant, τ, and initial speed, U_0. Glide distance, *d*, was measured at the mean glide duration for all fish (broken grey line). (C) Changes in speed are drawn according to measured parameter values entered into the speed equation for each fish (Eqn 3). (D–F) The mean (filled circles) and distribution (± 1 S.D.) of kinematic parameters plotted against the body length (*L*) for each fish. Orange, purple and green points correspond to the same individuals shown in panels A–C.

Table 2. *Dead drag measurements for a fish body length of 27.4±1.4 mm*

Re	*U* (mm s^{-1})	Dextran concentration (% of mass)	μ (10^{-3} kg m^{-1} s^{-1})	ρ (kg m^{-3})	*D* (μN)	C_{inert}	C_{visc}
1.33±0.41	0.85±0.26	7.92	18.9	1086	2.30±0.74	16.7±6.9	5.27±0.72
11.1±1.9	4.91±0.78	7.50	13.1	1081	10.2±2.8	2.04±0.56	5.82±1.39
75.3±8.1	13.7±1.3	4.73	5.22	1050	11.7±2.6	0.316±0.101	6.07±1.51
268±13	11.9±0.4	0.46	1.22	1005	2.10±0.42	0.077±0.012	5.37±0.92
994±62	36.4±1.4	0	1.00	1000	16.9±6.4	0.064±0.021	16.8±5.9
1560±70	57.1±2.3	0	1.00	1000	48.5±11.4	0.077±0.019	31.1±7.3
4910±250	215±1	0	1.20	1000	793±422	0.086±0.043	112±58
7780±400	341±1	0	1.20	1000	1510±340	0.066±0.010	135±25
12,100±630	530±2	0	1.20	1000	3560±1090	0.064±0.014	203±54

Re, Reynolds number; *U*, flow speed; μ, dynamic viscosity; ρ, density; *D*, drag; C_{inert}, inertial drag coefficient; C_{visc}, viscous drag coefficient. Values are means ± 1 S.D. (*N*=6).

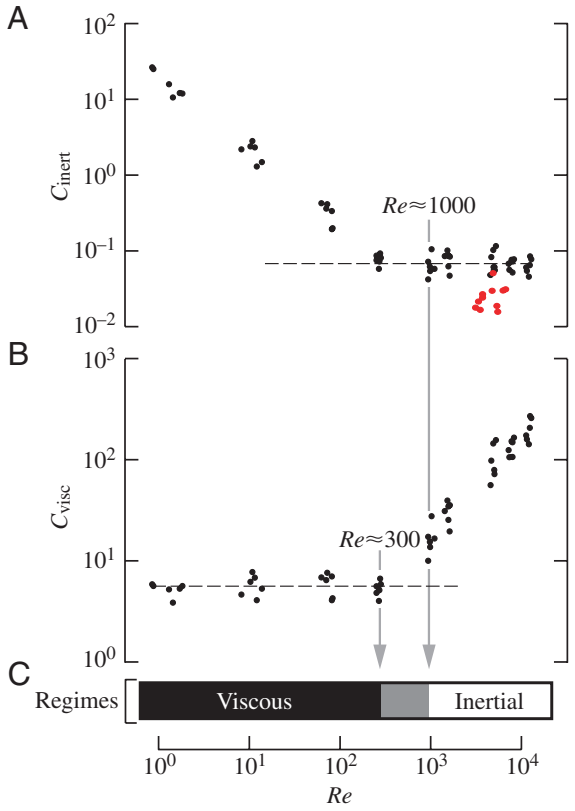

Fig. 5. Drag coefficient measurements and hydrodynamic regimes for adult zebrafish. Black circles denote dead drag measurements from tethering experiments (N=6; nine Re values per individual) and red circles are *in vivo* drag measurements (N=4; three coasts per individual). (A) The broken line lies at the mean value for the inertial drag coefficient (C_{inert}) at Re>1000. (B) The broken line denotes the mean value of the viscous drag coefficient (C_{visc}) at Re<300. (C) The viscous regime occurs where C_{visc} remains relatively constant, and the inertial regime is defined as the range where C_{inert} does not vary with Re.

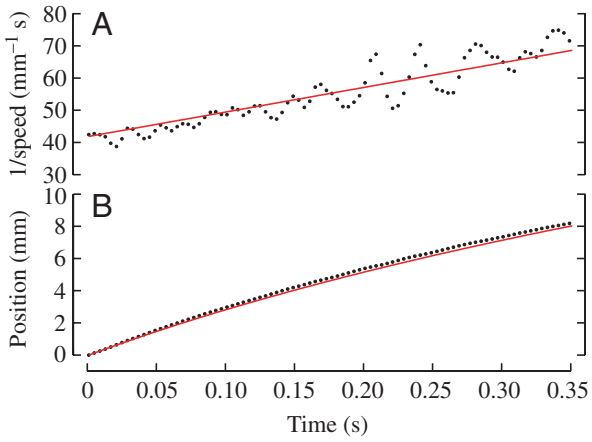

Fig. 6. Measurement of *in vivo* drag in a coasting fish at Re_{max}=1050. The inertial drag coefficient for this fish (L=25 mm) was calculated from measurements of body mass and surface area and (A) the inverse of instantaneous speed measurements during coasting (filled circles). The drag coefficient (C_{inert}=0.05) was found from a least-squares linear fit (red line) to the data, which (B) provided a prediction (red line) for the measured changes in the cranial position (filled circles).

between 1 and 10,000 (Table 2). The inertial drag coefficient varied across the 1<Re<1000 range, but remained relatively constant (C_{inert}=0.067±0.006; N=6; five Re values per fish) at higher Re values (Fig. 5A). By our criteria for hydrodynamic regimes (see Introduction), the range of Re where the inertial drag coefficient remained constant (Re>1000) defines the inertial regime. The viscous regime was defined at Re<300 because it is in this range that the viscous drag coefficient maintained a constant value (C_{visc}=5.72±0.41; N=6; three Re values per fish; Fig. 5B). The intermediate hydrodynamic regime was therefore found to be 300<Re<1000 (Fig. 5C). Differences in values for the drag coefficients at Re≈300 (C_{visc}=5.37±0.84, N=6; C_{inert}=0.064±0.019, N=6) and at Re≈1000 (C_{visc}=16.83±5.42, N=6; C_{inert}=0.076±0.011, N=6) were small (<0.1%) relative to the range of measured coefficient values (Fig. 5A,B).

We found differences between indirect and direct measurements of drag. The mean value (± 1 S.D.) for the inertial drag coefficient from *in vivo* measurements (C_{inert}=0.024±0.011; N=4; three glides per fish; Fig. 6) was nearly one-third the dead drag value for adult fish at Re>1000 (Fig. 5A). This is a highly significant difference (P<0.001), according to a two-tailed, unpaired Student's t-test (Sokal and Rohlf, 1995). Although significant, this discrepancy between methods of drag measurement is small (<0.2%) relative to the range of C_{inert} spanned across the Re values examined (Fig. 5A).

Drag measurements were related to the routine locomotion of fish by measuring the range of instantaneous Re values exhibited during coasting. The upper and lower limits of this range were progressively greater at larval, juvenile and adult stages (Fig. 7A). Small larvae generally ranged from Re≈1 to Re≈100 during coasting, whereas large adults spanned from Re≈1000 to Re≈10,000 (Fig. 7B). Larval and juvenile fish primarily operated at Re values within the viscous regime defined by our drag measurements (Fig. 5). By contrast, adult fish (L>23 mm) primarily operated in the inertial regime.

Mathematical models were used to examine the influence of scaling in hydrodynamics and momentum on coasting kinematics. Model fish operating in the same hydrodynamic regime travelled further if they had greater momentum at the start of the coast (Fig. 8). For example, when we created a model with the body size of a larva and the momentum of an adult, it traversed more than 100 times the length-specific distance in 0.5 s of a model with the momentum of a larva (Fig. 8A). A similar pattern was predicted for model fish the size of juveniles and adults (Fig. 8B–D). When momentum was held constant, model fish of larger body size encountered greater drag and therefore coasted less far. For instance, a model having the momentum and size of a large juvenile (green lines in Fig. 8C) coasted about half the length-specific distance of the same model reduced to the size of a larva (green lines in Fig. 8A).

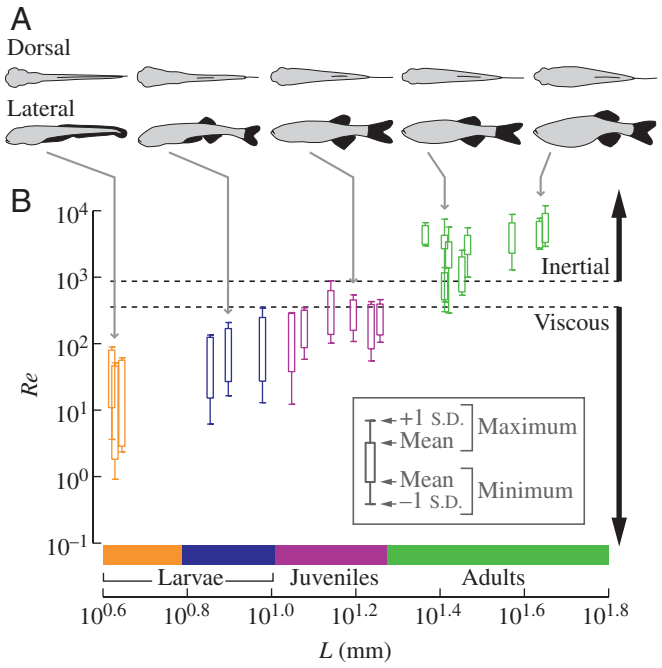

Fig. 7. Reynolds numbers (*Re*) spanned during coasting by zebrafish of different size. (A) Dorsal and lateral silhouettes illustrate the shape of the body (grey) and fins (black) at different stages of growth. (B) The range of *Re* traversed during coasting in fish of different size. The upper and lower edges of vertical bars and error flags denote, respectively, the mean and 1 S.D. of maximum and minimum values (as shown in key) for three coasts per fish (N=22). Stages of growth are colour coded for small larvae (orange), large larvae (blue), juveniles (purple) and adults (green). The hydrodynamic regimes (broken lines) from drag measurements (Fig. 5) are shown to the right.

Greater body mass and initial speed endows adults with more momentum at the beginning of a coast than juveniles, but adults also have a larger body size for drag to act upon. Direct comparisons of the mechanics of juvenile and adult stages are complicated by our finding that they operate in different hydrodynamic regimes (Figs 5, 7). Therefore, mathematical simulations were useful for differentiating the mechanical changes occurring during growth from juvenile to adult stages. Model fish coasted less far with the body size and inertial drag of adults (Fig. 8D) than with the size and viscous drag of juveniles having the same initial momentum (Fig. 8C). Simulations run within the viscous regime predicted that model fish the size of juveniles (Fig. 9A) coasted further than models the size of adults (Fig. 9B), and this effect was more pronounced in coasts of longer durations. A shift from the viscous to inertial hydrodynamics resulted in even shorter predicted coast distance (Fig. 9C), which suggests that the ontogenetic increase in coast distance (Fig. 4D) is not generated by changes in hydrodynamics. However, increasing body mass and initial speed to adult values (Fig. 9D,E) greatly increased predicted coast distance, which suggests that differences in momentum are dominant in determining the change in coast distance between juveniles and adults (Fig. 4D). Regardless of parameter values in these simulations, the differences between predictions that included the acceleration reaction were negligibly different from simulations that did not (Figs 8, 9).

Discussion

How does coasting performance change with size?

Our measurements of gliding kinematics over the full range of growth stages revealed nonlinear changes in performance over ontogeny. The most surprising of these changes was the large increase in coast distance and initial speed in the growth between juvenile and adult stages (Fig. 4D,E). On average, juveniles begin gliding at one-third the length-specific speed and travel less than half the length-specific distance of adults.

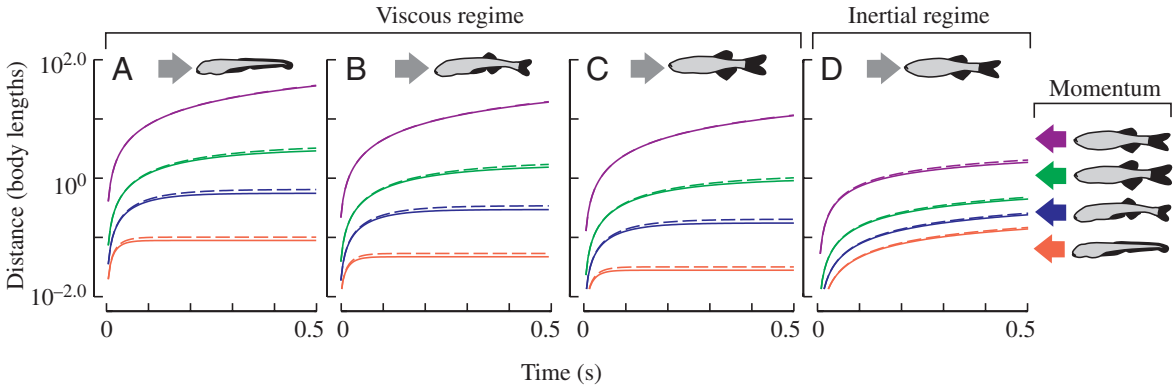

Fig. 8. The influence of momentum and hydrodynamics on coasting performance. Coasts were simulated using the mean parameter values for four ontogenetic stages. Simulations used the momentum, p, of adults (p=1.04×10^{-4} kg m s^{-1}; purple), juveniles (p=8.05×10^{-7} kg m s^{-1}; green), large larvae (p=8.28×10^{-8} kg m s^{-1}; blue) and small larvae (p=7.01×10^{-9} kg m s^{-1}; orange). Model coasting that included (solid line) and excluded (broken line) the added mass is shown. (A–C) Curves show the predicted change in body position as a function of time for coasting simulations in the viscous regime (Eqn 4), with the body lengths of (A) small larvae (L=4.35 mm), (B) large larvae (L=8.19 mm) and (C) juveniles (L=13.81 mm) shown. (D) Simulations of coasting in the inertial regime (Eqn 8) with the wetted surface area of adults (S=660 mm^2) were run at each level of momentum.

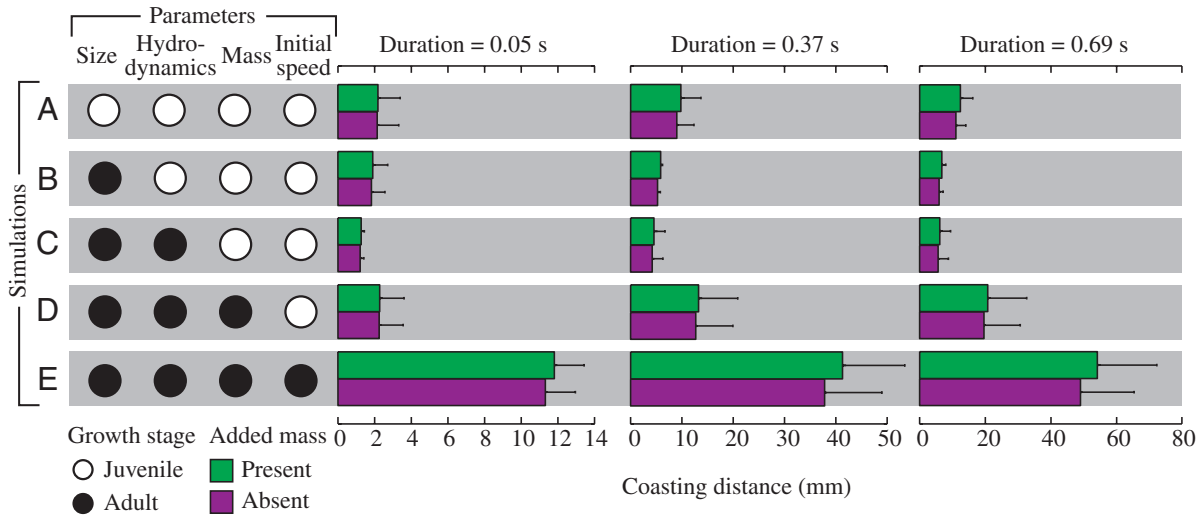

Fig. 9. The effects of mechanical parameter values on coasting distance in juveniles and adults. Coasting distances were calculated (Eqns 4, 8) for three glide durations in five simulations having unique parameter combinations. Simulations were run for each of the three measured juvenile and adult parameter values. The length of bars shows the mean (± 1 S.D.) of these predictions. (A,B) Predictions were generated from the position function for the viscous regime (Eqn 4) using body length as the size parameter. (A) The values for juvenile fish were used for all four parameters in this simulation. (B) Model fish were scaled to the length of adults in these simulations. (C,D) Predictions of coasting distance were calculated from the position function for the inertial regime (Eqn 8) using wetted surface area as the size parameter. (C) The effect of hydrodynamic regime alone may be assessed by comparison with B. (D) The model fish in these simulations were given the mass of adults. (E) All parameters were set at the measured adult values in these simulations.

Furthermore, the time constant gradually increased during growth to four times the value of larvae (Fig. 4F).

Our findings that adult zebrafish coast disproportionately further and faster, and maintain their speed for a longer duration than larvae and juveniles (Fig. 4D–F) are consistent with prior studies (e.g. Fuiman and Webb, 1988; Hunter, 1972; Muller et al., 2000). Our method of calculating coasting distance at an equivalent coast period (using Eqn 4) accounts for the small discrepancies between the values that we report and those of Muller et al. (2000) and Fuiman and Webb (1988). Furthermore, the 'resting period' data used in prior studies included time that fish spent motionless whereas our measure of coast duration included only the period of deceleration and therefore was of smaller value.

How do the hydrodynamics of coasting change with size?

The hydrodynamic scaling suggested by our measurements of dead drag does not agree with some previous studies on fish locomotion. We found that viscous forces dominate the generation of drag at Re<300, which has an upper limit that is more than an order of magnitude greater than that proposed by Weihs (1980) and considered by others (e.g. Fuiman and Webb, 1988; Muller and Videler, 1996; Osse, 1990; Osse and Drost, 1989; Videler, 1993; Webb and Weihs, 1986). Furthermore, the lower limit of our measured inertial regime (Re≈1000) is greater than what many have suggested (e.g. Osse and Drost, 1989; Videler, 1993; Webb and Weihs, 1986; Weihs, 1980), which leaves an intermediate transition over a relatively narrow range of Reynolds numbers (300<Re<1000) and drag coefficient values (Fig. 5). The scaling proposed by Weihs (1980) was reasonable because it was consistent with drag measurements of rigid bodies in the 1<Re<1000 range from the engineering literature (e.g. Hoerner, 1965). However, measurements at this scale have primarily focused on bluff bodies of spherical or cylindrical shape, with relatively little attention paid to streamlined bodies (although an abundance of research has examined the hydrodynamics of streamlined bodies at higher Re values; Hoerner, 1965). Our results suggest that the scaling of drag for a coasting fish is not well approximated by measurements of bluff bodies. This conclusion is perhaps not surprising given that bluff bodies exhibit separation and a turbulent wake within this scale, while airfoils at higher Re with a zero angle of attack generate little turbulence (Granger, 1995).

The hydrodynamic regimes defined by our drag measurements are entirely consistent with the results of Fuiman and Batty (1997). That study found that a linear relationship between stride length and the viscous drag product ($UL\mu$) in anchovy was disrupted at Re>300, which was interpreted as evidence of inertial drag and lead to the conclusion that fish are viscous-dominated at Re<300. Our results support this conclusion and raise the possibility that the scaling of drag examined presently may apply to the propulsive phase as well. Although the drag coefficient of a swimming fish is different from that of a coasting fish (Anderson et al., 2001; Blake, 1983; Drucker and Lauder, 1999; Schultz and Webb, 2002; Videler, 1981, 1993; Webb, 1975), drag may vary with Re in a similar manner for both phases. This hypothesis is at odds with the mathematical model of propulsion proposed for ascidian larvae by McHenry et al. (2003), which suggested a negligible contribution of viscous drag at Re≈100 during body undulation.

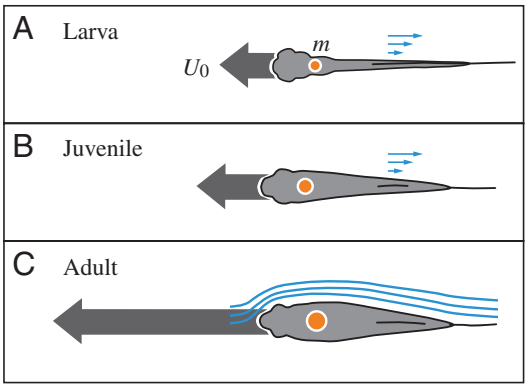

Fig. 10. Schematic diagram of the major changes in coasting dynamics over ontogeny. Larval (A) and juvenile (B) stages operate in the viscous regime (symbolized by a blue flow gradient), whereas the adult stage (C) operates in an in inertial regime (denoted by the blue streamlines). Despite this change in hydrodynamics, it is primarily the body mass (orange circle) and initial speed (grey arrow) that cause the observed differences in coasting performance (Fig. 4).

However, it is expected that the spherical trunk of an ascidian larva should more closely resemble the hydrodynamics of a bluff body and therefore have a lower limit to its viscous regime than the relatively streamlined body of a fish (McHenry, 2005). Computational fluid dynamics modelling verified with experimental measurements (e.g. Liu et al., 1996; Wolfgang et al., 1999) holds promise for examining differences in the scaling of drag between coasting and propulsive phases.

The present approach of expressing hydrodynamic scaling in terms of regimes is useful for interpreting large-scale ontogenetic change but has the danger of concealing physically important phenomena. For example, it is informative that drag varies directly with speed and not to its second power in juvenile fish. However, it would be inaccurate to predict that larvae and juvenile fish should generate identical flow fields because they both operate in the viscous regime. Inertia is present and dynamically relevant at low *Re*, and viscosity is required for generating turbulence at high *Re*. Furthermore, drag coefficients may vary with *Re* within regimes, although to a lesser degree than observed across regimes (Fig. 5). Hydrodynamic regime categorization provides a useful first-order approximation of dominant hydrodynamic forces but is limited in its ability to predict the flow fields that generate those forces or higher-order effects. Nonetheless, our results provide an empirical basis for verifying new experimental and theoretical approaches for understanding hydrodynamics at this scale.

Our measurements of drag coefficient are comparable to values reported in prior studies. Numerous studies have examined the inertial drag coefficients (usually denoted C_d) of the rigid bodies of adult fish and marine mammals at $Re>1000$. Employing a variety of experimental techniques, this literature reports values for C_{inert} ranging from 0.0034 to 5.59 (reviewed by Blake, 1983; Videler, 1993; Webb, 1975). Webb's dead drag measurements of *Salmo gairdneri* (L=300 mm, $3000<Re<20{,}000$; Webb, 1970) come close in body morphology to those of zebrafish. Our mean *in vivo* measurement of C_{inert}=0.024 is of comparable magnitude to Webb's mean of C_{inert}=0.036 (Webb, 1970). Despite a difference in body shape, computational simulations of dead drag in frog tadpoles (Re=7200) by Lui et al. (1997) also predicted a similar value (C_{inert}=0.0287).

Although measurements of *in vivo* drag have been restricted to the inertial regime in the present study, a method for measuring drag in larval and juvenile fish is apparent from our results. The time constant found by a non-linear curve fit to position data (using Eqn 4) or velocity data (using Eqn 3) is inversely proportional to the viscous drag coefficient. As long as a coasting fish is operating in the viscous regime, measurements of time constant, body length, mass and body volume may be used to calculate the viscous drag coefficient with Eqn 11. Although no comparable equations exist for fish operating in the intermediate regime ($300<Re<1000$), our finding that the C_{inert} varies little in this range suggests that methods for measuring C_{inert} *in vivo* (e.g. Bilo and Nachtigall, 1980) provide a reasonable approximation for coasting in this regime.

Discrepancies between dead drag and *in vivo* measurements of drag coefficient demonstrate the limitations on what may be interpreted from dead drag experiments. The range of C_{inert} values spanned in the $1<Re<10{,}000$ range (Fig. 5A) far exceeded (by more than a factor of 5000) the difference between *in vivo* and dead drag measurements. However, we did find that tethered adult fish generated nearly three times the drag of freely coasting fish. Possible sources for this difference include chemical fixation (which presumably alters the mechanics of mucus and surface compliance) or differences in the posture of the fins or angle of attack between the bodies of dead and live fish. Although this discrepancy appears minor in the context of hydrodynamic scaling, a threefold difference in drag may be substantial for considerations of the energetics of locomotion. Our results should therefore contribute to scepticism about the application of dead drag as an absolute measurement of force coefficients for physiological studies (Schultz and Webb, 2002).

Our mathematical modelling suggests that the added mass of the surrounding water does not make a meaningful contribution to the dynamics of coasting zebrafish. The coasting distances predicted in models that included the added mass were negligibly different from those that did not (Figs 8, 9). This result is not surprising, given that the added mass was assumed to be equal to that of a 1:6 ellipsoid, which is a geometry that accelerates a relatively small volume of fluid (Kochin et al., 1964; Munk, 1922). Furthermore, a coasting body does not generate the large oscillatory accelerations created during the propulsive phase, where acceleration reaction is expected to play a much larger role in hydrodynamics (Lighthill, 1975; Wu, 1971). However, it remains possible that the added mass could contribute to coasting dynamics if the added mass coefficient was at a comparable magnitude to what Webb (1982) found in the fast-starts of trout.

How does the scaling of drag and momentum affect performance?

Although the hydrodynamic changes occurring over the life history of zebrafish are dramatic, our results suggest that changes in coasting performance are largely driven by the scaling of momentum (Fig. 10). Our mathematical model predicted that the increase in relative coast distance from juvenile to adult stages is actually hindered by the transition from viscous (Fig. 9B) to inertial (Fig. 9C) regimes. This detrimental consequence of hydrodynamics is overcome by an increase in momentum between these stages. The greater mass and, especially, the faster initial speed propel the body of an adult disproportionately further (Fig. 9). High initial speed may be the result of reduced drag production from the more streamlined body shape of adults (Fig. 7A), or adults may be more effective at generating thrust. The end result is that the scaling of performance in the coasting phase is largely dictated by the performance of the propulsive phase.

Mechanical scaling and ontogenetic change

Our results present an opportunity for new interpretations of ontogenetic changes in the behaviour of fish. The newly hatched larvae of zebrafish (Buss and Drapeau, 2001) and other species of comparable size (Hunter, 1972; Osse and van den Boogaart, 2000) routinely swim in relatively long bouts at steady speed but shorten the duration of the propulsive phase and swim more intermittently as they grow to a size that routinely operates at Re>30. During the transition towards more intermittent swimming, some fish appear to develop greater manoeuvrability, as the curvature of tail beating decreases while maintaining or enhancing their ability to change direction (Fuiman and Webb, 1988; Muller and van Leeuwen, 2004; Osse and van den Boogaart, 2000). A number of studies have suggested that intermittent swimming and greater manoeuvrability are consequences of operating in a more inertial hydrodynamic environment (e.g. Fuiman and Webb, 1988; Webb and Weihs, 1986; Weihs, 1980). However, our results indicate that the viscous regime extends into Re of more than an order of magnitude greater than assumed by these analyses, which suggests that these behavioural transitions may not be attributed to a hydrodynamic regime change. Furthermore, we found that coasting performance is better predicted by ontogenetic changes in momentum than the scaling of drag. This suggests that even a revised consideration of hydrodynamic scaling must be coupled with the inertial dynamics of the body in order to accurately evaluate the functional significance of ontogenetic change in behaviour, especially in fish that swim intermittently.

Patterns of morphological change during growth may be more a reflection of developmental or historical constraints than an adaptation to changing hydrodynamic conditions. Zebrafish, like many fish species, have an elongated body at hatching but gradually develop a more compressed and streamlined shape during larval and juvenile growth (Osse, 1990; Webb and Weihs, 1986). Investigators have posited that this elongated shape allows larvae to precociously exit the viscous regime by having a greater body length, and therefore higher Re, than if they distributed their mass in a streamlined form. According to this hypothesis, juveniles gradually abandon an elongated shape after exiting the viscous regime in order to reduce drag by streamlining as they grow into an increasingly inertial environment (Fuiman and Webb, 1988; Muller and Videler, 1996; Osse, 1990; Osse and Drost, 1989; Sagnes et al., 2000; Webb and Weihs, 1986). However, our results suggest that these changes in body shape occur well within the viscous regime (Re<300). The fusiform body shape of adults is probably an adaptation for locomotion, but it develops in juvenile zebrafish before coasting can benefit from the inertial drag reduction that comes from streamlining (Fig. 3). Given that an elongated larval body is the plesiomorphic condition in the Chordata (Berrill, 1955; McHenry and Patek, 2004; Stokes, 1997), it is more plausible that this morphology is a developmentally or historically constrained trait rather than an adaptation to locomotion (as in jellyfish; McHenry and Jed, 2003). Furthermore, an elongated shape may facilitate gas exchange or other physiological functions (Liem, 1981; Webb and Weihs, 1986), which suggests that stabilizing selection may have acted in the evolution of aquatic vertebrates to retain this ancestral condition.

List of symbols

A	added mass coefficient
a	body acceleration
C_{inert}	inertial drag coefficient
C_{visc}	viscous drag coefficient
d	coast distance
D	measured drag
h	slope of the inverse of speed *vs* time
L	body length
m	body mass
p	momentum
Re	Reynolds number
S	wetted area of the body
t	time
U	speed
U_0	initial speed
V	body volume
φ	angular fin position
μ	water dynamic viscosity
θ	cranial orientation
ρ	water density
τ	time constant

We thank E. Tytell, T. Hsieh, J. Liao, J. Roman, A. Summers, W. Korff, and S. Patek for their input on the manuscript. W. Korff provided critical technical advice. This work was supported by a NSF Postdoctoral Research Fellowship to M.J.M. and NSF grant IBN0316675 to G.V.L. P. Webb and an anonymous reviewer provided valuable feedback.

References

Anderson, E. J., McGillis, W. R. and Grosenbaugh, M. A. (2001). The boundary layer of swimming fish. *J. Exp. Biol.* **204**, 81-102.

Batchelor, G. K. (1967). *An Introduction to Fluid Dynamics*. New York: Cambridge University Press.

Berrill, N. J. (1955). *The Origin of Vertebrates*. Oxford: Clarendon Press.

Bilo, D. and Nachtigall, W. (1980). A simple method to determine drag coefficients in aquatic animals. *J. Exp. Biol.* **87**, 357-359.

Blake, R. W. (1983). *Fish Locomotion.* Cambridge: Cambridge University Press.

Budick, S. A. and O'Malley, D. M. (2000). Locomotor repertoire of the larval zebrafish: Swimming, turning and prey capture. *J. Exp. Biol.* **203**, 2565-2579.

Buss, R. R. and Drapeau, P. (2001). Synaptic drive to motoneurons during fictive swimming in the developing zebrafish. *J. Neurophys.* **86**, 197-210.

Clark, B. D. and Bemis, W. (1979). Kinematics of swimming penguins at the Detroit Zoo. *J. Zool. Lond.* **188**, 411-428.

Daniel, T., Jordan, C. and Grunbaum, D. (1992). Hydromechanics of Swimming. In *Advances in Comparative and Environmental Physiology*, vol. 11 (ed. R. M. Alexander), pp. 17-49. London: Springer-Verlag.

Drucker, E. G. and Lauder, G. V. (1997). Aquatic propulsion in fishes by vortex ring production. *Am. Zool.* **37**, 77A.

Drucker, E. G. and Lauder, G. V. (1999). Locomotor forces on a swimming fish: Three-dimensional vortex wake dynamics quantified using digital particle image velocimetry. *J. Exp. Biol.* **202**, 2393-2412.

Fuiman, L. A. and Batty, R. S. (1997). What a drag it is getting cold: Partitioning the physical and physiological effects of temperature on fish swimming. *J. Exp. Biol.* **200**, 1745-1755.

Fuiman, L. A. and Webb, P. W. (1988). Ontogeny of routine swimming activity and performance in zebra danios (Teleostei: Cyprinidae). *Anim. Behav.* **36**, 250-261.

Granger, R. A. (1995). *Fluid Mechanics*, 2nd edn. New York: Dover Publications.

Hoerner, S. F. (1965). *Fluid-Dynamic Drag.* Brick Town, NJ: Hoerner Fluid Dynamics.

Hunter, J. R. (1972). Swimming and feeding behavior of larval anchovy *Engraulis mordax*. *Fish. Bull.* **70**, 821-838.

Johansson, C. L. (2003). Indirect estimates of wing-propulsion forces in horizontally diving Atlantic puffins (*Fratercula artica* L.). *Can. J. Zool.* **81**, 816-822.

Johnston, T. P., Cullum, A. J. and Bennett, A. F. (1998). Partitioning the effects of temperature and kinematic viscosity on the c-start performance of adult fishes. *J. Exp. Biol.* **201**, 2045-2051.

Kochin, N. E., Kibel, I. A. and Roze, N. V. (1964). *Theoretical Hydrodynamics*. New York: John Wiley & Sons.

Lamb, H. (1945). *Hydrodynamics*, 6th edn. New York: Dover Publications.

Lang, T. G. and Daybell, D. A. (1963). Porpoise performance tests in a seawater tank. *Nav. Ord. Test Sta. Tech. Rep.* **3063**, 1-50.

Lathi, B. P. (1998). *Signal Processing and Linear Systems*. New York: Oxford University Press.

Liem, K. F. (1981). Larvae of air-breathing fishes as countercurrent flow devices in hypoxic environments. *Science* **211**, 1177-1179.

Lighthill, J. (1975). *Mathematical Biofluidynamics.* Philadelphia: Society for Industrial and Applied Mathematics.

Lighthill, M. J. (1971). Large-amplitude elongated-body theory of fish locomotion. *Proc. Roy. Soc. Lond. B* **179**, 125-138.

Liu, H., Wassersug, R. J. and Kawachi, K. (1996). A computational fluid dynamics study of tadpole swimming. *J. Exp. Biol.* **199**, 1245-1260.

Liu, H., Wassersug, R. and Kawachi, K. (1997). The three-dimensional hydrodynamics of tadpole locomotion. *J. Exp. Biol.* **200**, 2807-2819.

McHenry, M. J. (2001). Mechanisms of helical swimming: asymmetries in the morphology, movement and mechanics of larvae of the ascidian *Distaplia occidentalis*. *J. Exp. Biol.* **204**, 2959-2973.

McHenry, M. J. (2005). The morphology, behavior, and biomechanics of swimming in ascidian larvae. *Can. J. Zool.* **83**, 62-74.

McHenry, M. J. and Jed, J. (2003). The ontogenetic scaling of hydrodynamics and swimming performance in jellyfish (*Aurelia aurita*). *J. Exp. Biol.* **206**, 4125-4137.

McHenry, M. J. and Patek, S. N. (2004). The evolution of larval morphology and swimming performance in ascidians. *Evolution* **58**, 1209-1224.

McHenry, M. J. and Strother, J. A. (2003). The kinematics of phototaxis in larvae of the ascidian *Aplidium constellatum*. *Mar. Biol.* **142**, 173-184.

McHenry, M. J., Azizi, E. and Strother, J. A. (2003). The hydrodynamics of locomotion at intermediate Reynolds numbers: undulatory swimming in ascidian larvae (*Botrylloides* sp.). *J. Exp. Biol.* **206**, 327-343.

Muller, U. K. and van Leeuwen, J. L. (2004). Swimming of larval zebrafish: ontogeny of body waves and implications for locomotory development. *J. Exp. Biol.* **207**, 853-868.

Muller, U. K. and Videler, J. J. (1996). Inertia as a 'safe harbour': Do fish larvae increase length growth to escape viscous drag? *Rev. Fish Biol. Fish.* **6**, 353-360.

Muller, U. K., Stamhuis, E. J. and Videler, J. J. (2000). Hydrodynamics of unsteady fish swimming and the effects of body size: Comparing the flow fields of fish larvae and adults. *J. Exp. Biol.* **203**, 193-206.

Munk, M. M. (1922). Notes on aerodynamic forces – I. Rectilinear motion. *Natl. Adv. Comm. Aeronaut.* **104**, 1-13.

Osse, J. W. M. (1990). Form changes in fish larvae in relation to changing demands of function. *Neth. J. Zool.* **40**, 362-385.

Osse, J. W. M. and Drost, M. R. (1989). Hydrodynamics and mechanics of fish larvae. *Pol. Arch. Hydrobiol.* **36**, 455-466.

Osse, J. W. M. and van den Boogaart, J. G. M. (2000). Body size and swimming types in carp larvae: effects of being small. *Neth. J. Zool.* **50**, 233-244.

Sagnes, P., Champagne, J. Y. and Morel, R. (2000). Shifts in drag and swimming potential during grayling ontogenesis: relations with habitat use. *J. Fish. Biol.* **57**, 52-68.

Schultz, W. W. and Webb, P. W. (2002). Power requirements for swimming: do new methods resolve old questions? *Integr. Comp. Biol.* **42**, 1018-1025.

Sokal, R. R. and Rohlf, F. J. (1995). *Biometry*. New York: W. H. Freeman.

Stokes, M. D. (1997). Larval locomotion of the lancelet *Branchiostoma floridae*. *J. Exp. Biol.* **200**, 1661-1680.

Thorsen, D. H., Cassidy, J. J. and Hale, M. E. (2004). Swimming of larval zebrafish:fin-axis coordination and implications for function and neural control. *J. Exp. Biol.* **207**, 4175-4183.

Videler, J. J. (1981). Swimming movements, body structure, and propulsion in cod (*Gadus morhua*). In *Vertebrate locomotion*, vol. 48 (ed. M. H. Day), pp. 1-27. London: Zoological Society of London.

Videler, J. J. (1993). Fish swimming. London: Chapman & Hall.

Videler, J. J., Stamhuis, E. J., Muller, U. K. and van Duren, L. A. (2002). The scaling and structure of aquatic animal wakes. *Integr. Comp. Biol.* **42**, 988-996.

Walker, J. A. (1998). Estimating velocities and accelerations of animal locomotion: a simulation experiment comparing numerical differentiation algorithms. *J. Exp. Biol.* **201**, 981-995.

Webb, P. W. (1970). Some aspects of the energetics of swimming fish with special reference to the cruising performance of rainbow trout. PhD dissertation, University of Bristol, UK.

Webb, P. W. (1975). Hydrodynamics and energetics of fish propulsion. *Bull. Fish. Res. Bd. Can.* **190**, 1-158.

Webb, P. W. (1982). Fast-start resistance of trout. *J. Exp. Biol.* **96**, 93-106.

Webb, P. W. and Weihs, D. (1986). Functional locomotor morphology of early life-history stages of fishes. *Trans. Am. Fish. Soc.* **115**, 115-127.

Weihs, D. (1980). Energetic significance of changes in swimming modes during growth of larval achovy, *Engraulis mordax*. *Fish. Bull.* **77**, 597-604.

Westerfield, M. (1995). The Zebrafish Book: A Guide for the Laboratory Use of Zebrafish, *Brachydanio rerio*. Eugene, OR: University of Oregon Press.

White, F. M. (1991). *Viscous Fluid Flow*. New York: McGraw-Hill.

Wolfgang, M. J., Anderson, J. M., Grosenbaugh, M. A., Yue, D. K. P. and Triantafyllou, M. S. (1999). Near-body flow dynamics in swimming fish. *J. Exp. Biol.* **202**, 2303-2327.

Wu, T. Y. (1971). Hydromechanics of swimming propulsion. Part 2. Some optimum shape problems. *J. Fluid Mech.* **46**, 521-544.

Wu, T. Y. (1977). Introduction to the Scaling of Aquatic Animal Locomotion. In *Scale Effects in Animal Locomotion* (ed. T. J. Peldley), pp. 203-232. London: Academic Press.